Synthesis of Cu NPs in a high-temperature jet mixing reactor

Authors: Priya Jana[a] and Nicholas Brunelli*[,a]

Author address: [a] The Ohio State University, William G. Lowrie Department of Chemical and Biomolecular Engineering, 151 W. Woodruff Ave., Columbus, OH 43210, U.S.A.

***Corresponding author:** Email: brunelli.2@osu.edu

Abstract

Scalable manufacturing of nanomaterials can enable capturing technological innovation from laboratory scale batch synthesis for commercial scale use. Yet, batch reactors in laboratories often struggle to produce consistent results, especially under scaled-up conditions because they fail to achieve rapid mixing. Rapid mixing is achieved in a scalable, high-temperature jet-mixing reactor (JMR) was employed to synthesize size-controlled copper (Cu) nanoparticles (NPs) that are monodisperse and reproducible. Using identical precursor concentrations, the JMR produced Cu NPs with an average diameter of (~10 nm), confirmed by TEM and DLS, and a narrow, monomodal surface plasmon resonance (SPR) peak in UV–Vis spectra. In comparison, batch synthesis under the same conditions yielded larger, polydisperse particles (~267 nm), consistent with non-uniform nucleation and growth. Whereas batch synthesis resulted in inconsistent UV-Vis spectra consistent with non-uniform particle formation between batches, it is determined that JMR had consistent performance over the duration of a single test and between different tests. Further tests scaling the batch synthesis resulted in a complex mixture whereas the JMR maintained consistent particle size and optical characteristics. These results demonstrate that the JMR enables scalable, reproducible, and monodisperse Cu nanoparticle synthesis, overcoming key limitations of traditional batch processing.

Keywords: Cu NPs, millifluidic reactor, mixing, jet mixing reactor

1. Introduction

Fundamental limitations associated with mixing impede the scaling up of batch processes, limiting our ability to use the remarkable properties discovered when synthesizing NPs in the research laboratory. Indeed, NPs have extensive applications ranging from catalysis,[1] drug delivery,[2] food processing,[3] and biomedical applications[4] because of their unique properties associated with their nanometer-scale dimensions. These small NPs have huge commercial implications in applications that demand precision in product quality (e.g., particle size uniformity). Over the past decade, many NPs such as gold, silver, and Cu have been extensively synthesized by wet-chemical reduction methods, chemical vapor deposition, and sol-gel methods with each of these methods corresponding to a batch process. Batch processes can be inexpensive and offer good control over the shape and size of the NPs until scaled up.[5] Yet, batch reactors are highly prone to batch-to-batch variability, a challenge that becomes exacerbated when scaling up production quantities. When the volume of the solvent and precursor concentration are scaled up, the synthesis conditions can lead to non-uniformity in the shape and size of the particles. These discrepancies primarily arise from the difficulties in maintaining uniform reaction conditions at larger volumes because of poor mixing.[6] Indeed, the effectiveness of mixing is the product of the reactor cumulative mixing time, which is the summation of the timescales for macromixing, mesomixing, and micromixing. For batch reactors, scaling the reactor size at minimum causes an increase in the macromixing time, resulting in an increase in the cumulative mixing time. Cumulative mixing times greater than the formation time of NPs lead to non-uniform mixing conditions. The non-uniform mixing and heat transfer rates in batch systems can lead to issues such as agglomeration and uncontrolled particle growth. These limitations have hindered the ability to scale up the quantity of nanomaterials and limit their usage in potential applications.

Accordingly, developing scalable nanomanufacturing methods requires additional research to enable capturing the full benefits of laboratory scale synthetic methods.

An alternative to a batch reactor is a millifluidic flow reactor. Millifluidic flow reactors have dimensions on the scale of millimeters with the active zone of the reactor being microliters in volume. The high surface area to volume ratio in mixing channels in a millifluidic reactor minimizes the effect of the macromixing time, reducing the overall mixing time compared to the formation time of NPs.[6] A millifluidic reactor could offer excellent reproducibility and less polydispersity because of its fast mixing and uniform heat and mass transfer conditions over batch processes. The uniform reaction conditions and fast mixing help to improve the scale-up of these NPs without compromising the product quality.

Researchers have investigated different types of millifluidic flow reactors, including a confined impinging jet mixer, a multi-inlet vortex mixer, and a jet-mixing reactor.[7] A confined impinging jet (CIJ) mixer was developed by Johnson and Prudhomme in 2003 to study flash nanoprecipitation induced by micromixing through combining a solvent containing dissolved polymer with a non-solvent.[8] The CIJ mixer provides rapid micromixing – as fast as 1.5 ms – but this level of rapid mixing requires equal momentum of the two inlet streams. For CIJ mixers, the equal momentum requirement results in the outlet stream having more than 50% of the antisolvent. This limits the extent of supersaturation happening in the mixing chamber.[7] To overcome this limitation a multi inlet vortex mixer (MIVM) was used to synthesize NPs that can use four jets with unequal momentum.[7] MIVM allows better flexibility to synthesize different sizes of NPs by changing the flow rates of the different streams.[9] However, it was observed from the numerical simulations studies that mixing is inferior in large MIVM compared to their small MIVM at high Reynolds number.[10] Jet mixing reactors (JMRs) are uniquely positioned as a promising solution for nanoparticle synthesis because of their ability to achieve rapid and uniform mixing, addressing many of the challenges associated with conventional reactor designs. These reactors use high-velocity fluid jets to create intense mixing, ensuring homogeneous reaction conditions within very short time scales.[11] This efficient mixing minimizes concentration gradients, allowing for precise control over nucleation and growth processes, which is critical for producing NPs with a narrow size distribution and low polydispersity.

JMRs have been used previously to synthesize NPs such as silicon NPs in the gas phase[12] and different NPs such as lipid and polystyrene NPs[13] and metal NPs like silver and gold NPs,[14] ZIF-8 NPs[15] in the liquid phase at room temperature. Compared to the batch process, all these synthesized NPs have reduced polydispersity and controlled growth when synthesized using the JMR. The JMR has also been used to synthesize the shell of core@shell NPs such as Pd@TiO_2, where batch synthesized Pd NPs are introduced in JMR for coating with TiO_2.[16] Whereas Pd@TiO_2 nanoparticle formation was performed in semi-batch since Pd nanoparticle formation requires high temperature, continuous synthesis of Au@Ag core@shell NPs[17] has been achieved. Although we have demonstrated synthesis of many different types and structures of nanomaterials, our previous work has focused on synthesis of nanomaterials at room temperature that are not strictly anhydrous or anaerobic. In this study, we will investigate the JMR operating at a high temperature and under inert conditions for the synthesis of NPs in liquid phase reactions so that we can create a continuous method to produce Pd@TiO_2 nanomaterials. As Pd is relatively expensive, we will focus on synthesizing Cu NPs as a model system for testing the robustness of the high temperature JMR as well as the inert conditions since Cu NPs are prone to oxidation that poses a challenge to synthesize the controlled shape and size of the particles.

Cu NPs are an intriguing model system since they have broad applications across various industries, including as catalysts for important reactions. Indeed, they are extensively used in the water-gas shift reaction, which plays a crucial role in hydrogen production.[18] Furthermore, their ability to act as catalysts in organic transformations, such as coupling reactions[19] and oxidation processes underscore their versatility and growing importance in chemical industries. As a transition metal, Cu exhibits an electronic configuration that facilitates the loss of electrons, typically forming oxidation states of +1 or +2, resulting in Cu_2O or CuO. Unlike noble metals Cu is highly prone to oxidation and dissolution, readily dissolving back to ionic precursors if not maintained under strictly inert conditions.[20] This instability of the particles makes it a stringent requirement to use an inert reactor set up, making Cu an effective probe of whether the JMR can sustain a reducing inert environment at elevated temperature.

In addition to their sensitivity to dissolved oxygen, Cu NPs have been produced through a variety of wet-chemical and batch-based synthesis methods. Reported batch processes span a wide range of conditions and particle sizes—for example, 28 nm Cu NPs formed using ascorbic acid at 80 °C, as well as shape- and size-dependent particles generated at 100–190°C in other studies. Beyond solution-phase routes, batch techniques such as chemical vapor deposition, reverse micelle synthesis, and atomic layer deposition have also yielded Cu NPs ranging from approximately 5 to 150 nm. Overall, these batch routes produce Cu NPs across diverse size regimes, but they commonly exhibit batch-to-batch variability and broad particle size distributions, reinforcing the need for more controlled reactor environments.

Our study addresses key limitations of the batch synthesis process, focusing on maintaining uniform PSD and minimizing the rapid oxidation of Cu NPs. We compare the particle properties between batch and continuous flow processes. Specifically, we investigate the performance of an inert high-temperature jet mixing reactor under different temperatures and flow rates, demonstrating its potential as a scalable pathway for producing these metallic NPs. The results indicate that the jet mixing reactor, with its efficient mixing time scales, produces Cu NPs with significantly smaller size and lower polydispersity than the batch process, highlighting its reliability and suitability for industrial applications. Overall, the work adds a new dimension for the scalable nanomanufacturing of using a jet-mixing reactor.

2. Experimental Methods

2.1. Chemicals

All chemicals were used as received, including Cu chlorine triphenyl phosphine (97%, 15709-76-9), tert-butylamine borane (TBAB) complex (97%, 7337-45-3; VWR), oleylamine (70%, O7805; Sigma Aldrich), oleic acid (Sigma Aldrich), ethanol (200 proof, Fischer Chemical), and toluene (HPLC grade, Fisher Chemical. The Cu precursor and tert-butylamine borane were stored in the glovebox under inert conditions.

2.2. Batch synthesis of Cu NPs

The synthesis procedure was completed in an inert atmosphere using Schlenk conditions or in a glovebox except for the centrifugation step. Cu chlorine triphenyl phosphine (0.15 g), and TBAB (0.21 g) were measured into separate three-neck round-bottom flasks (RBF) fitted with condensers capped with a septum and septa on the other two necks. After removing from the glovebox, the RBFs were attached to the Schlenk line and purged with nitrogen for 15 minutes. In a third RBF, toluene (50 mL) was degassed with nitrogen. After degassing, toluene (15 mL) was added to the RBF with the Cu precursor and 17 mL was added to the RBF with the TBAB reducing agent. Both were degassed with nitrogen for another hour. Both the RBFs were placed in oil baths, and the temperature was set to 100°C. Once the desired temperature was reached, oleyl amine (250 μL) was added to the Cu solution, and the mixture was stirred for 5 minutes. The reducing agent solution was transferred to the Cu solution, and a reddish-brown color was observed, indicating the formation of NPs. After adding the reducing agent, the mixture was heated at 100°C for an hour. The solution was reddish brown in color, consistent with the Cu solution being reduced by TBAB. After an hour, the solution was cooled to room temperature, and oleic acid (400 μL) was added and stirred for 5 minutes. The solution was then mixed with degassed ethanol (15 mL), transferred to a centrifuge tube, and centrifuged for 10 minutes at 8000 rpm. The washing and centrifugation procedure was repeated twice, and the precipitate was dispersed in toluene for further characterization.

2.3. Continuous synthesis of Cu NPs using a heated jet mixing reactor

The continuous flow heated jet mixing reactor (JMR) was constructed in-house and comprised a stainless-steel pre-heating block and a separate heated JMR block. The pre-heating block consisted of two plates (5 in. length × 4 in. width × 0.5 in. height) that were sandwiched together using bolts. On the inside faces, the blocks had three internal channels that accommodate the main and jet inlet lines (all three lines are 1/16” tubing). Both the preheating unit and the JMR were equipped with cartridge heaters inserted into bores drilled perpendicularly into the block. The temperature was controlled using an Omega PID controller that used a K-type thermocouple inserted into a hole drilled into the block at the geometric center as well as a second PID controller with a K-type thermocouple inserted into the geometric center of the JMR. The

cartridge heaters were cartridge heaters with standard lead wire covering for 1/8’ hole, 120 V AC, 2’’ long heating element and 100 W specifications. Similar to our previous work, the reactor inlet configuration was comprised of one main line and two jet lines.[14] The main line was fabricated with an internal diameter of 0.04 in. (100 µm), while the two opposing jet lines had internal diameters of 0.02 in (50 µm) with the two jet lines impinging perpendicularly into the main channel. The combined stream exits the reactor parallel to the main line. The reactant solutions were delivered using two PHD 2000 Infusion (Harvard Apparatus) syringe pumps.

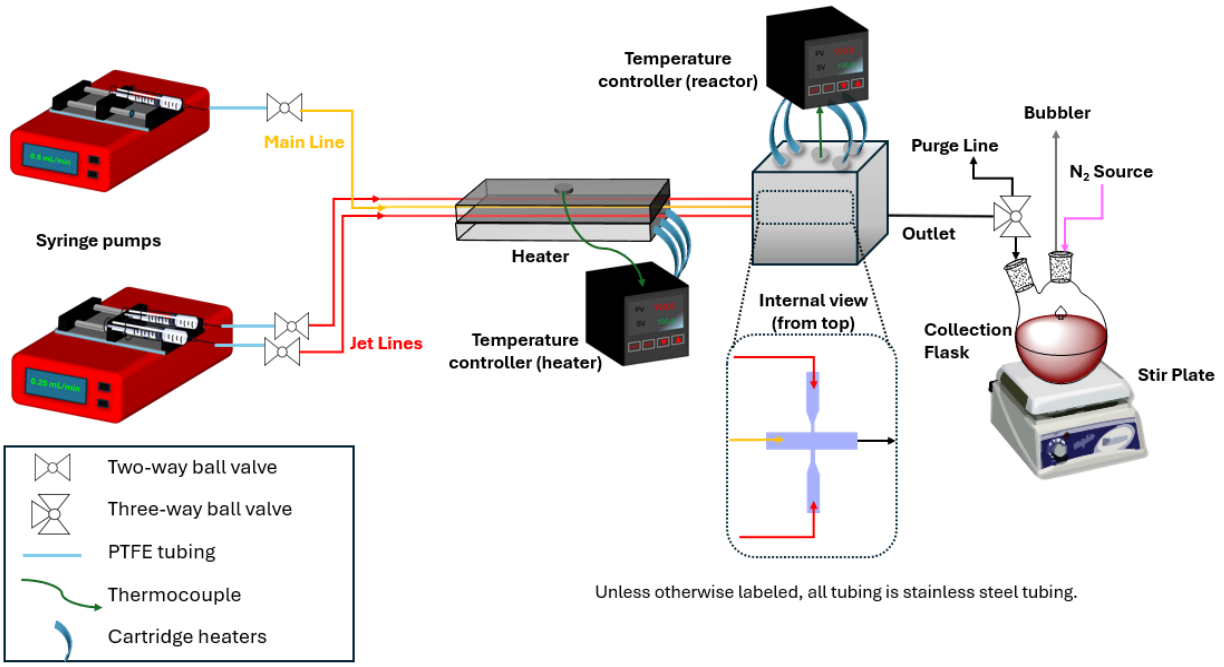

Scheme 1. Schematic of the high temperature JMR for the synthesis of Cu NPs that includes syringe pumps for delivering the precursors, a feedback-controlled heater, a JMR with integrated feedback-controlled heating, and a collection flask.

The outlet of the reactor was connected to a three-way valve that could be directed to one of two RBFs. The reactor was purged through connecting a nitrogen line from a Schlenk line was connected to one RBF. With no direct path for the outlet flow to leave the flask, the nitrogen flows through the system backwards from the flask towards the reactor. The entire reactor setup was flushed with nitrogen for 20 minutes. This process was repeated for the second RBF so that both collection flasks are maintained under inert conditions.

Before starting the synthesis, the pre-heater and reactor were heated through turning on the temperature controllers with the temperature set at 100°C. While heating and purging, the Cu precursor and TBAB inside the glovebox were measured separately in two three-necked RBFs attached to a condenser. All the necks of the RBFs were sealed with rubber septum. Both flasks were degassed under nitrogen for 15 minutes. Degassed toluene (15 mL) was added to the RBF with the Cu precursor and 17 mL were injected into the RBF with TBAB. The RBFs were heated at 100°C under an inert nitrogen atmosphere. Once the Cu precursor reaches the desired temperature, oleylamine (520 µL) was added to the Cu precursor, which was then stirred at 400 rpm for five minutes. The Cu solution was loaded in a 25 mL Luer lock syringe that was placed into one syringe pump. The TBAB solution was loaded into two separate syringes of 25 mL in equal volume in a second syringe pump. The Cu solution was connected to the main line of the reactor and the reducing agent to the jet lines of the reactor. The pump was operated at a main line flow rate of Q_{main} = 0.8 mL min^{-1} and jet line flow rate of Q_{jet} = 0.4 mL min^{-1}. Oleic acid (400 µL) was added to the RBF at the outlet of the reactor and stirred continuously while the solution was collected. The solution was then mixed with degassed ethanol (15 mL), transferred to centrifuge tubes, and centrifuged for 15

minutes at 8000 rpm. The supernatant was discarded, and the precipitate was redispersed in degassed toluene (5 mL) for characterization.

2.4. Material characterization

After the precipitate is redispersed in toluene, the particle size and size distribution were studied by Dynamic Light Scattering (DLS) and Transmission Electron Microscopy (TEM). DLS was measured using a Malvern Zetasizer Pro Light Scattering instrument. The sample was added to a glass cuvette with 10 µL of product solution diluted with 1 mL of toluene. In addition, samples for TEM are prepared by drop casting 7.5 µL of sample on 400-mesh carbon film Cu grids. The grids were kept in Petri dishes and dried in an oven overnight at 80 °C to remove organic from the sample. TEM samples were imaged using a FEI Tecnai G2 Spirit Transmission Electron Microscopy at a voltage of 80 kV and magnification of 115,000x in bright field mode. The particle size analysis was performed using ImageJ software. UV-Vis analysis was performed using an Evolution Pro spectrophotometer (Thermo Scientific). Degassed toluene (1 mL) was taken as a blank in a quartz cuvette. The Cu solution (200 µL) was then added in the cuvette, and the spectrum for the sample was recorded after 10 minutes.

3. Results and discussion

3.1. Batch Synthesis

A batch method was used to synthesize Cu NPs using a method that is similar to previous reports.[24] The method involved wet chemical reduction of a Cu precursor with a constant reducing agent-to-Cu precursor ratio and using a temperature of 100 °C. After injecting the reducing agent into the RBF with the Cu precursor, we observed a color change with the solution becoming reddish-brown. This promising observation was tempered after adding ethanol to precipitate the Cu NPs (NPs). The reddish-brown solution changed to a green solution with limited to no precipitate. Despite using similar conditions, each separate batch produced inconsistent results as to whether a precipitate formed or did not form. When a precipitate formed, it was re-dissolved in toluene and analyzed using UV-Vis. As shown in (**Figure 1)**, the spectrum had a peak near 320 nm that was consistent with CuO NPs. Whereas limited attention had been placed on dissolved oxygen in the solvents, it appeared that the oxygen dissolved in ethanol transformed the Cu NPs into Cu oxide (CuO) NPs. When using identical synthesis conditions except for degassing ethanol, it was observed that after adding degassed ethanol, the reddish-brown color was still present. The solution was centrifuged, resulting in formation of a precipitate. The precipitate was redispersed in toluene, and the solution was analyzed using UV-Vis. The resulting spectrum had a peak around 600 nm that is associated with the surface plasmon resonance (SPR) of Cu NPs, consistent with the presence of Cu NPs (**Figure 1**).

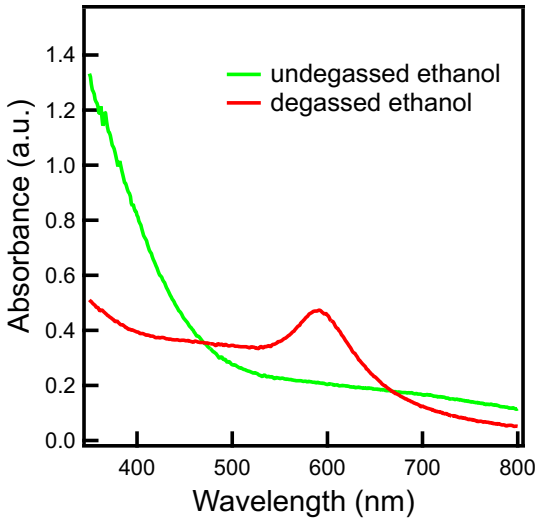

Figure 1. UV-Vis spectrum of Cu NPs synthesized using a batch method at 100 °C, followed by precipitation with ethanol that either had or had not been degassed.

As UV-Vis data were consistent with Cu NPs, the materials were evaluated using DLS and TEM to determine the particle size and PSD. DLS measurements showed a mean hydrodynamic particle size of approximately 310 nm from both the intensity vs. size (**Figure 2**) and number vs. size (**Figure 2**) for the Cu NPs in dispersion. Both distributions consistently show that the majority of Cu NPs are larger than 100 nm, showing consistency between the two analyses.

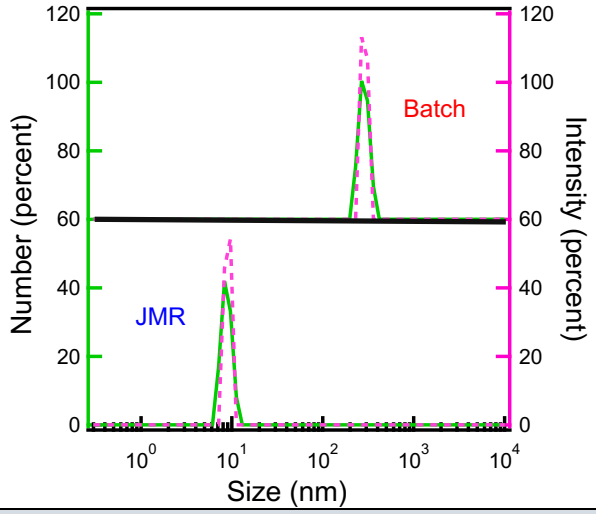

Figure 2. DLS showing number percent and intensity percent vs size for Cu NPs synthesized in batch and JMR at 100 °C.

TEM was used to corroborate the particle size and to determine the structure of the Cu NPs. From multiple sections of the TEM grid, images were recorded that showed the particle size and structure with a representative image presented in (**Figure 3a)**. The image contained particles with a primary size of ~300 nm that were clustered together to form agglomerates. ImageJ analysis was performed on more than 200 particles to obtain a PSD. From these data, it was determined that the primary particles had a mean particle diameter of 250 nm (**Figure 3b)**, which NPs are larger than the target particle size of <100 nm. The large particle size could be due to inefficient mixing in batch processes. It was also noted that the particles were agglomerated with many large Cu NPs forming into large aggregates, which would be a limitation for processes requiring dispersed NPs.

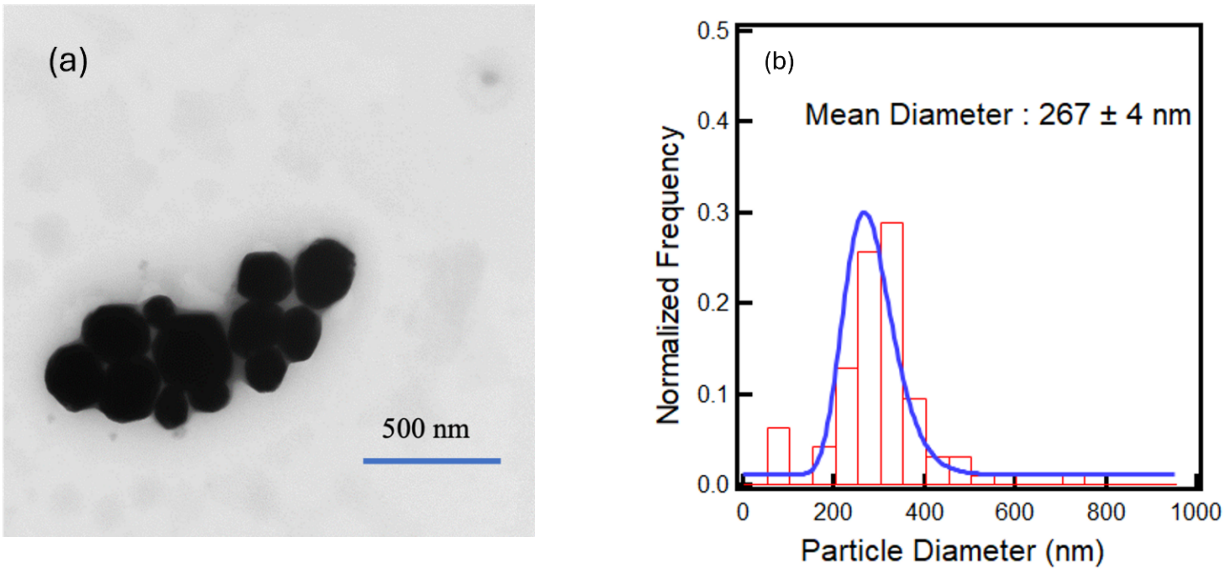

Figure 3. (a) TEM image of Cu NPs synthesized in batch at 100°C. (b) ImageJ analysis of Cu NPs synthesized in batch at 100°C.

The reproducibility of batch synthesis of Cu NPs was evaluated through using a combination of repeated experiments and temporal evaluation of the synthesis mixture. When repeating experiments, the synthesis method used ethanol that had been degassed. These repeated runs (1 to 4) were evaluated using UV-Vis (**Figure 4a)**. The UV-vis data were fit using the curve fitting routine in Igor using the Gauss fit, as illustrated in **Figure S1**. In spite of efforts to produce consistent materials, it was observed that the UV-Vis adsorption spectra had distinct peaks and intensities for each run, as listed in **Table S1** (in Supplemental Information). The peak location varied from 573 to 595 nm. The average peak value was 587 nm with a standard deviation of ±10 nm. The value of the standard deviation demonstrated that the batch synthesis method produced materials with properties that varied considerably between batch. In addition, it was determined that the full-width at half maximum (FWHM) for the Gaussian fit ranged from 38 to 80 nm. The average value for the FWHM of different runs was 67 nm with a standard deviation of 20 nm, further demonstrating that the batch methods produce results that vary significantly between batches. These results showed one challenge with scalable manufacturing of Cu NPs with batch processes.

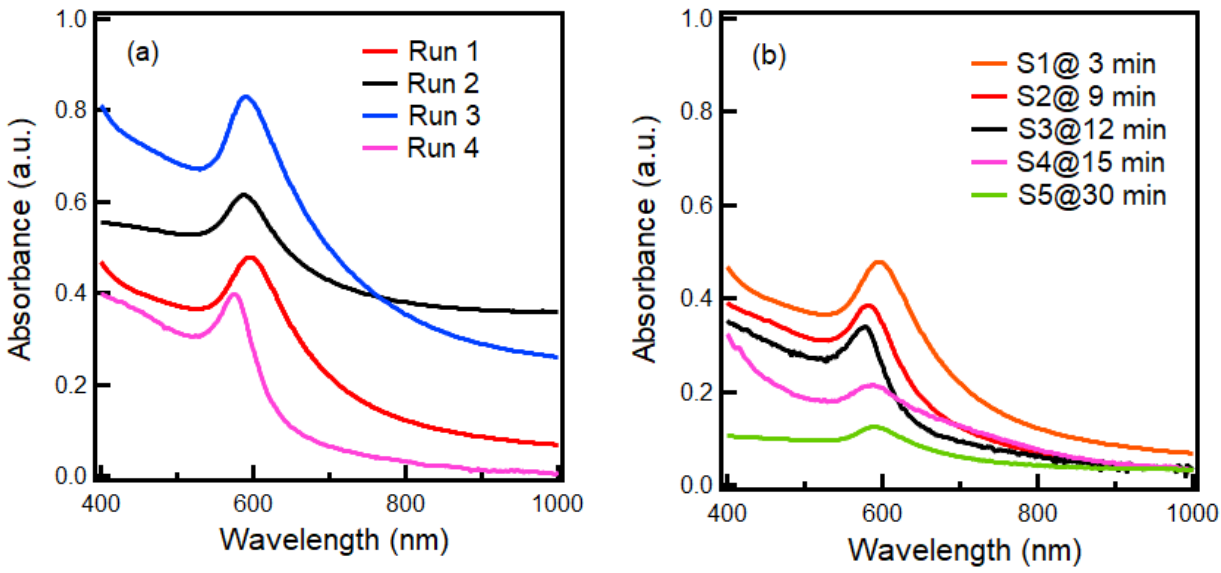

Figure 4. (a) UV-Vis spectra of Cu NPs synthesized at 100 °C taken from different batch runs and (b) taken at different time instances from a single batch run.

From the repeated experiments, it was noted the solution changed color rapidly, suggesting that the NPs formed rapidly and may not require an hour to form, as had been used previously.[24] Accordingly, the synthesis was followed temporally through taking aliquots at specific time points **Figure 4(b)**. Samples were taken at different time intervals for 3, 9, 12, 15, and 30 min. Interestingly, the absorption spectrum for the 3-minute sample had a sharp peak located at 594 nm with a FWHM of 73 nm. With increasing time, the absorption peak red-shifted to 589 nm, decreased intensity, and broadened with a FWHM of 118 nm around 30 mins. These observations were consistent with uncontrolled growth and aggregation. Scaling these processes would likely result in batch-size dependent properties and would require repeated optimization at each production scale to maintain consistent particle sizes and uniform size distributions.

These results highlighted the challenge that synthesis of Cu NPs posed and were reasons that we selected Cu NPs as the model system for testing continuous synthesis of NPs in a heated and inert JMR. As an alternative, we tested JMR as a method to synthesize uniform-shaped and sized NPs in an inert, high-temperature environment. Whereas our previous work[14] with a JMR had focused on room temperature synthesis under ambient conditions, adapting the current synthesis of Cu NPs using a JMR required modifying the system to be able to operate under inert conditions at high temperature.

3.2 JMR synthesis of NPs

As an alternative, Cu NPs were synthesized using a JMR through adapting the batch synthesis process. The JMR was operated at 100 °C with flow rates of Q_{main} = 0.8 mL min^{-1} and Q_{jet} = 0.4 mL min^{-1}. The JMR had two opposing jets through which Q_{jet} = 0.4 mL min^{-1} for a total Q_{jets} = 0.8 mL min^{-1}. Correspondingly, these conditions were termed symmetric flow conditions.

Particles synthesized in JMR were characterized using UV-Vis, DLS, and TEM. The UV-Vis spectra showed a distinct difference in both the peak position and FWHM between the batch and JMR samples, as shown in **Figure 5**. These UV-vis data for JMR synthesized NPs were fit similar to how the UV-vis data for batch synthesized data were fit. The JMR sample exhibits a SPR peak at 575.5±0.2 nm that had a FWHM of 43±1 nm. The sharp peak was consistent with the formation of small and monodisperse NPs**.**

In contrast, the batch sample showed a red-shift and broader peak at 595 nm with a FWHM of 74 nm, consistent with batch processes forming particles with a larger size and broader size distribution than the particles synthesized in JMR.

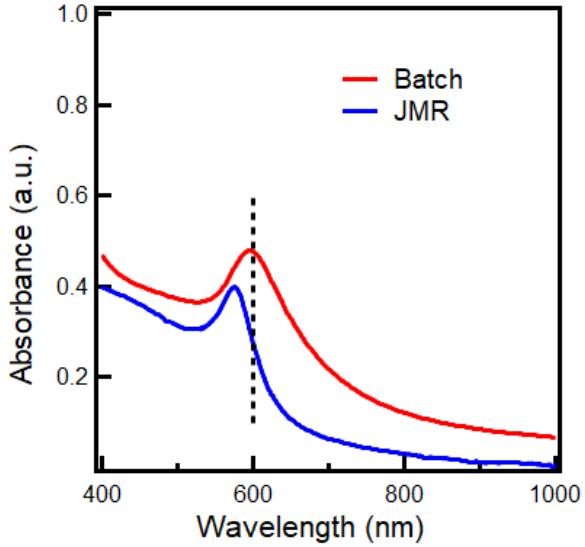

Figure 5. Comparison of UV-Vis properties of Cu NPs synthesized at 100 °C using a batch method and the JMR at a flow rate of Q_{main} = 0.8 mL min^{-1} and Q_{jet} = 0.4 mL min^{-1} .

The particle size and PSD of the particles synthesized in JMR was further confirmed by DLS and TEM. For Cu NPs synthesis using the JMR, both the intensity percent (**Figure 2**) and number percent size graph (**Figure 2**) in DLS had a peak that corresponded to particles with a diameter of around 9.9 nm for Cu NPs synthesized in JMR. ImageJ analysis of 248 particles synthesized in JMR (**Figure 6 (a)**) showed a mean PSD of around 10 nm (**Figure 6 (b)**), consistent with DLS results. The particle size synthesized in JMR confirmed by DLS and TEM is around 25 times smaller than that of batch synthesis.

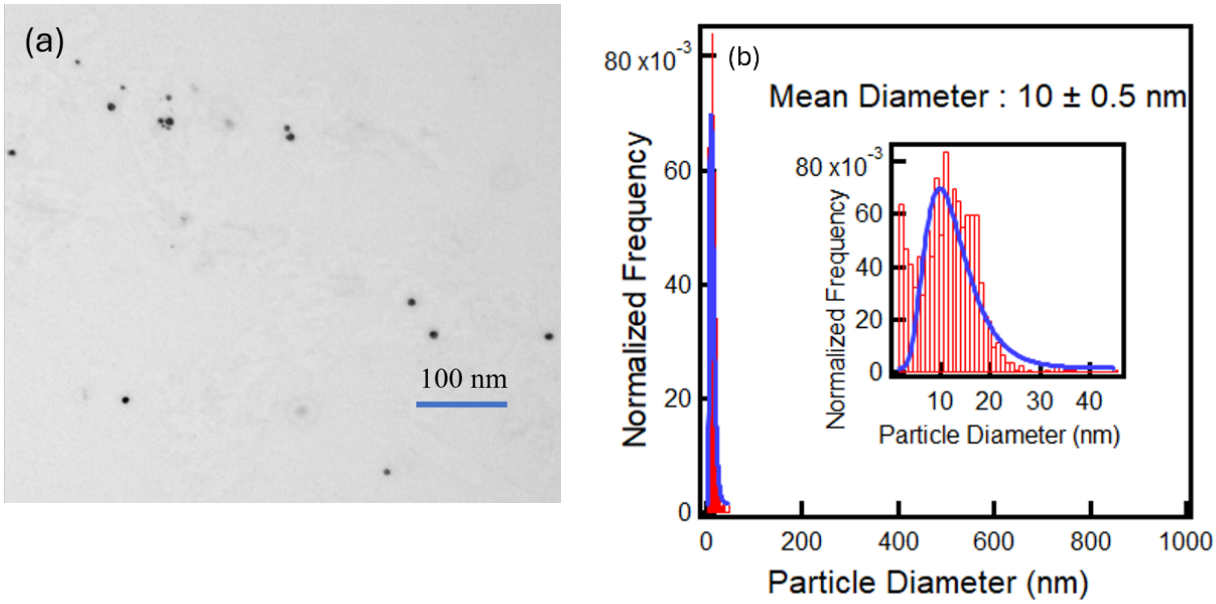

Figure 6. (a) Representative TEM image of Cu NPs synthesized in JMR at 100 °C at Q_{main} = 0.8 mL min^{-1} and Q_{jet} = 0.4 mL min^{-1}. (b) Image J analysis of 248 Cu NPs synthesized in JMR at 100 °C at Q_{main} = 0.8 mL min^{-1} and Q_{jet} = 0.4 mL min^{-1}.

The reproducibility of the JMR was also tested for the synthesis of Cu NPs in JMR at standard conditions at 100°C at Q_{main} = 0.8 mL min^{-1} and Q_{jet} = 0.4 mL min^{-1}. The evolution of Cu NPs was monitored using UV-Vis spectroscopy. Samples were taken from the RBF at the outlet at 3 min, 9 min, 12 min, 15 min and 30 min, and UV-Vis spectra of the samples were collected (**Figure 7(a)**). The peak positions remained nearly constant with time, consistent with uniform particle formation. Compared to batch process (**Figure 4(b)**), the FWHM was markedly narrower, 37 nm, demonstrating that the particles are monodisperse. The reproducibility was also tested across different synthesis runs, and it was observed that the peaks almost overlap with each other from Run 1 to Run 4 (**Figure 7(b)**). Overall, the JMR achieves reproducible reaction conditions, yielding NPs with nearly identical sizes and narrow distributions, independent of run-to-run variations.

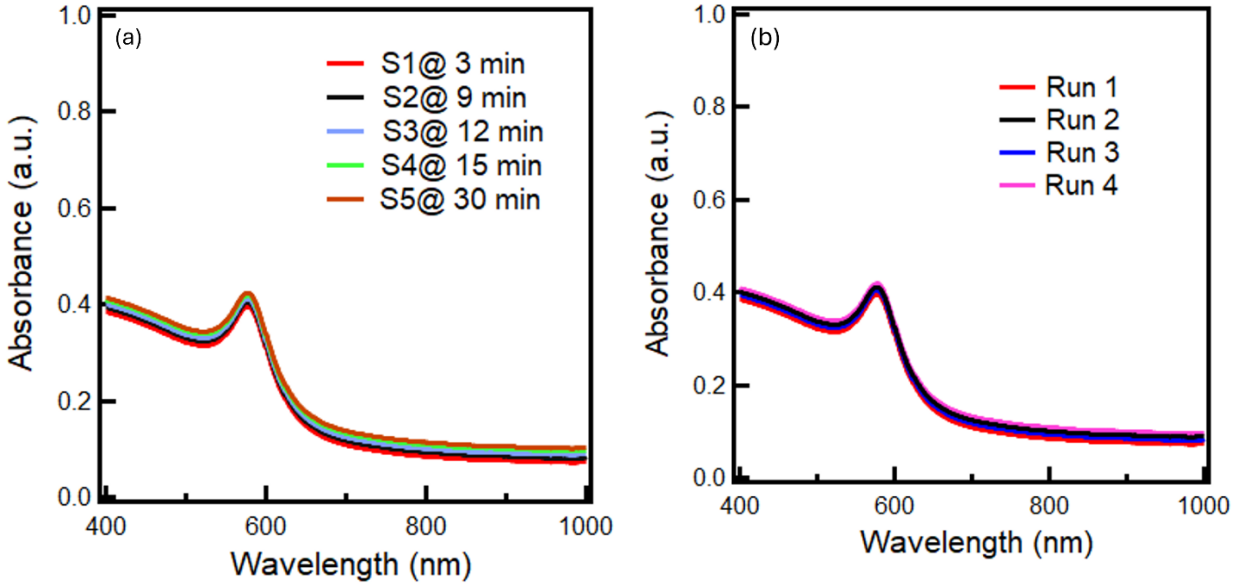

Figure 7. (a) UV-Vis spectrum of Cu NPs synthesized at 100 °C taken at different time instances from a single JMR run and (b) taken from different JMR runs

3.2.1. Effect of flow rate on particle size synthesized in jet-mixing reactor

After establishing the reproducibility of the JMR for producing Cu NPs, the range of potential operating conditions are evaluated. The JMR was operated at different flow rates. Compared to the original conditions, we reduced the flow rate to Q_{main} = 0.4 mL min^{-1} and Q_{jet} = 0.2 mL min^{-1}. The reduced flow rate would reduce mixing intensity and increase residence time. As shown in **Figure 8**, the particle sample had a UV-Vis spectra that had a red shift compared to the standard flow conditions (i.e., Q_{main} = 0.4 mL min^{-1} and Q_{jet} = 0.2 mL min^{-1}), corresponding to larger sized particles at lower flow rate.

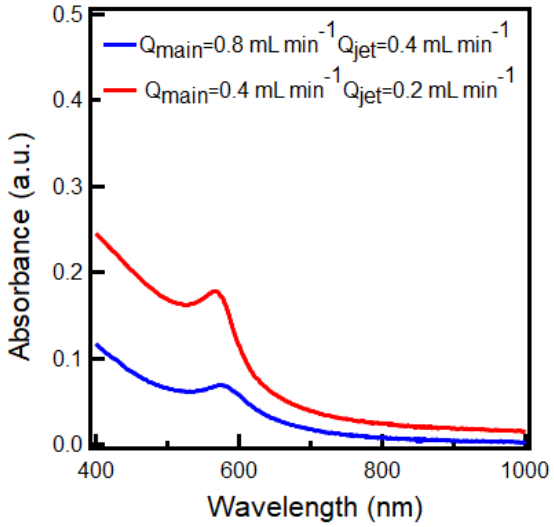

Figure 8. Comparison of the UV-Vis spectra of Cu NPs synthesized using different flow rates in the JMR at 100°C.

The sample was collected and imaged with TEM, as shown in **Figure 9**. The sample was determined to have small particles as well as Cu nanorods. Compared to higher flow rates, the particles are larger, around 18 nm in size, from TEM analyzed in Image J analysis (**Figure 10**). This is also confirmed by the intensity vs size (**FigureS1**) and number vs size (**Figure S2**) graph from DLS, where the mean particle size is 18.5 nm. These results were reproducible when using the same reaction conditions. The increase in particle size was attributed to the increase in residence time. Whereas the residence time would be a straightforward parameter to vary to tune particle size, the formation of nanorods would limit operation at these conditions.

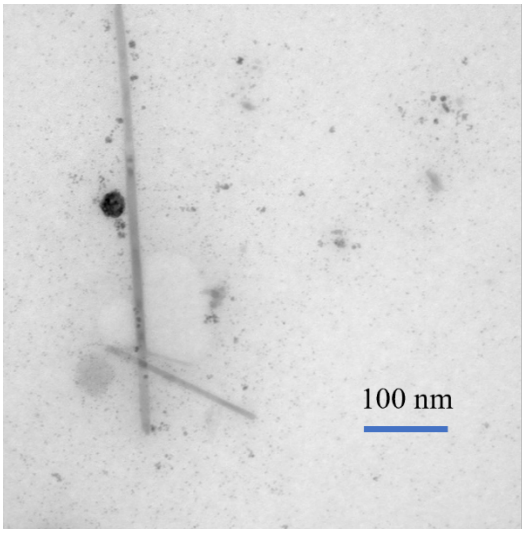

Figure 9. TEM image of Cu NPs synthesized in JMR at 100 °C at Q_{main} = 0.4 mL min^{-1} and Q_{jet} = 0.2 mL min^{-1}.

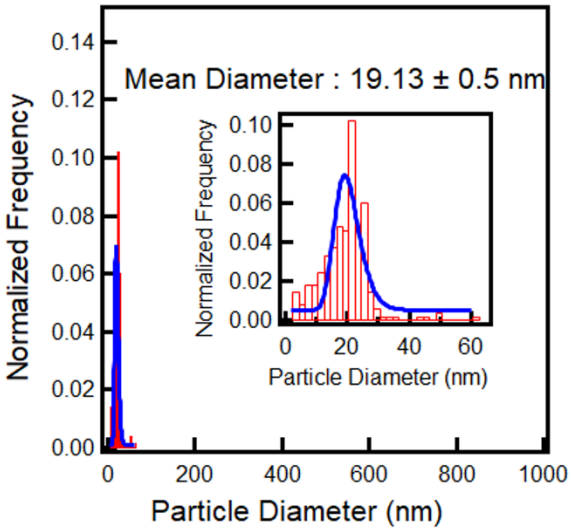

Figure 10. Image J analysis of Cu NPs synthesized in JMR at 100 °C at Q_{main} = 0.4 mL min^{-1} and Q_{jet} = 0.2 mL min^{-1} scale.

In addition to reducing the flow rate, the JMR was tested at an increased flowrate of Q_{main} = 1 mL min^{-1} and Q_{jet} = 0.5 mL min^{-1}. At this flow rate, the mixing time would be expected to be reduced, leading to uniform reactant distribution and local supersaturation. This would result in increased

nucleation where small particles would be increase in number rather than large ones. Yet, when operating the JMR at a flow rate Q_{main} = 1 mL min^{-1} and Q_{jet} = 0.5 mL min^{-1}, no noticeable change of color was observed in the solution at the outlet of the reactor, indicating no particles were formed. This result suggested that Cu NPs requires a minimum residence time for the reducing agent to reduce the Cu precursor. This would be an important consideration when scaling up the productivity of the JMR.

3.2.2. Effect of pre-heating temperature on the synthesis of Cu nanoaprticles in JMR

In addition to the flow rates, we speculated that the temperature would strongly impact the resulting materials. These temperatures included the solution temperature before loading into the syringe ($T_{Solution}$), the solution temperature of the liquid loaded in the syringe ($T_{Syringe}$), the pre-heater (T_{Heater}), and the JMR (T_{JMR}). These different temperatures were assessed to check the impact on nanoparticle formation.

When considering the different temperatures, we tested the hypothesis that preheating of the solution was required. Rather than pre-heating the solution and loading the syringe with heated liquid, the solutions were mixed and loaded into the syringe at room temperature (i.e., $T_{Solution}$ = $T_{Syringe}$ = room temperature) while setting T_{Heater} and T_{JMR} at 100 °C. Oleylamine was added to the Cu solution at room temperature and the JMR was operated at a flow rate of Q_{main} = 0.8 mL min^{-1} and Q_{jet} = 0.4 mL min^{-1}. For these conditions, the synthesis did not produce a precipitate, indicating no particle formation consistent with our hypothesis that preheating of the solution is required.

The temperature was increased for $T_{Solution}$ = $T_{Syringe}$ = 80 °C while maintaining the T_{Heater} and T_{JMR} at 100 °C. Oleylamine was added at 80 °C to the Cu solution in the RBF. The JMR was operated at standard synthesis conditions at a flow rate of Q_{main} = 0.8 mL min^{-1} and Q_{jet} = 0.4 mL min^{-1}. For these conditions, the solution was collected in the RBF at the outlet and had a reddish-brown color. The material was centrifuged resulting in a reddish-brown precipitate, indicating formation of Cu NPs. The precipitate was re-dispersed in degassed toluene and characterized using UV-Vis, DLS, and TEM. The presence of a peak around 600 nm indicates the presence of Cu (**Figure S3**). DLS showed a particle size around 300 nm both in intensity vs. size (**Figure S4**) and number vs. size (**Figure S5**) graphs. This is consistent with the Cu NPs shown in TEM (**Figure 11**) where particles appear agglomerated. Compared to the standard synthesis conditions where the synthesized Cu NPs were monodispersed and smaller in size the above condition produced large agglomerates of Cu NPs.

It is unclear why $T_{Solution}$ and $T_{Syringe}$ have such a marked impact on particle formation. It is noted that heating the precursor solution was widely reported for nanoparticle synthesis when using oleylamine. It is speculated that heating helps to facilitate the coordination of the oleylamine with the Cu precursor, making it susceptible for reducing to induce. It would be possible that this exchange only partially happened at lower temperature. For the current work, this result demonstrated the importance of pre-heating the reactants to the reactor temperature.

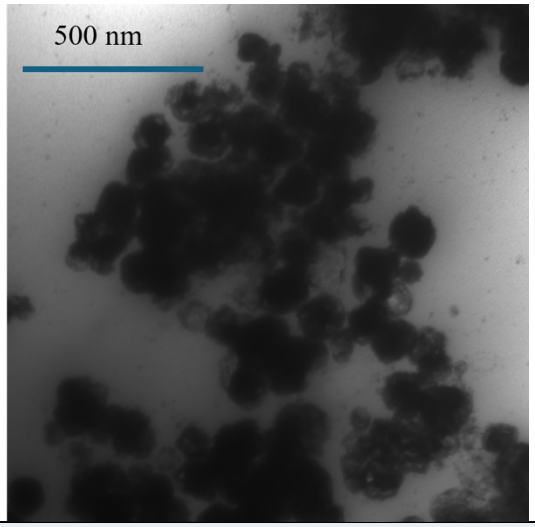

Figure 11. TEM of Cu NPs synthesized in JMR at modified conditions showing agglomerates are formed.

3.3. Scaling up of NPs in batch and JMR processes

An important aspect of commercialization is scaling up the production quantity of NPs while maintaining a uniform shape and size. When maintaining all other reaction conditions constant, the precursor volume was scaled up threefold [Cu solution: 51 mL; TBAB solution: 45 mL]. The presence of a peak around 600 nm shows the successful synthesis of copper both in batch (**Figure S6**) and JMR processes (**Figure S7**). For the batch process, the synthesis resulted in the desired color change of solution, forming the desired precipitate. The samples were analyzed with TEM to evaluate particle dispersity. TEM analysis showed heterogeneity across different regions of the grid. Some areas contained spherical NPs with an average diameter of ~14 nm (**Figure 12(a)**), but other regions had agglomerated structures (**Figure 12(b)**). The lack of uniformity was corroborated by DLS measurements. It was observed in the DLS data of intensity vs. size (**Figure 12(c)**) that two PSDs were present: a smaller peak at 20 nm and a larger peak at 200 nm, consistent with the particles being highly agglomerated. These results were distinct from the small-scale synthesis and demonstrate that the particle properties synthesized in batch depend on synthesis scale. This non-uniformity in shape and size would make the batch process non-ideal for scaling up the batch process.

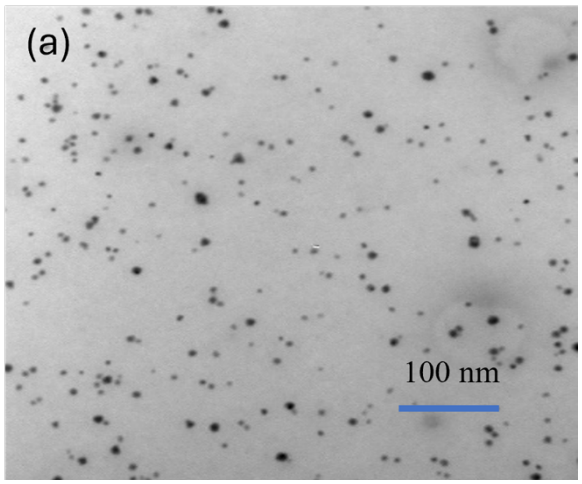

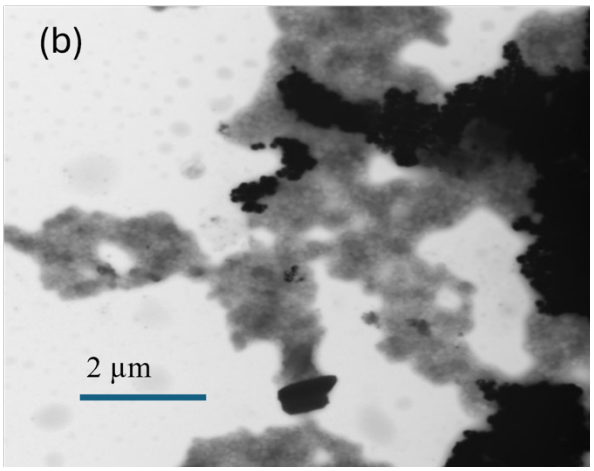

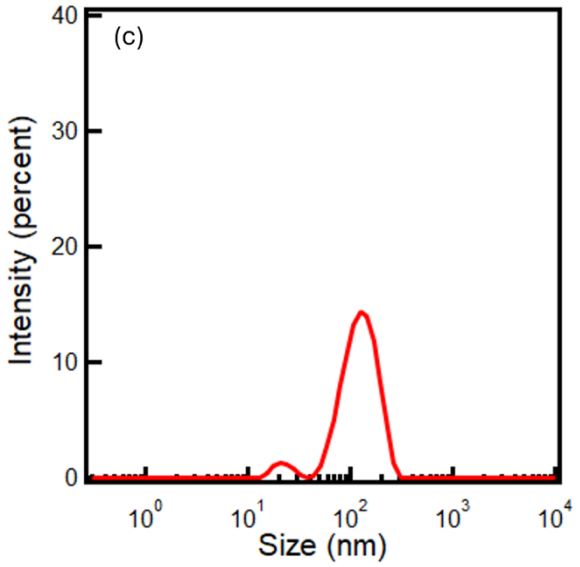

Figure 12. (a) TEM images of Cu NPs synthesized in scaled up batch process at 100 °C. (b) TEM images of Cu NPs from a different section of the TEM grid in scaled up batch processes at 100 °C. (c) Intensity vs. size graph from DLS for Cu NPs synthesized in batch at 100 °C.

The scalability of JMR synthesis was demonstrated through scaling up the precursor quantity and operating the JMR at Q_{main} = 0.8 mL min^{-1} and Q_{jet} = 0.4 mL min^{-1} at a temperature of 100 °C. Under these conditions, the NPs remained highly uniform and spherical as seen in TEM (**Figure 13(a)**). Image J analysis showed the average size of these particles to be ~9.9 nm (**Figure 13(b)**).

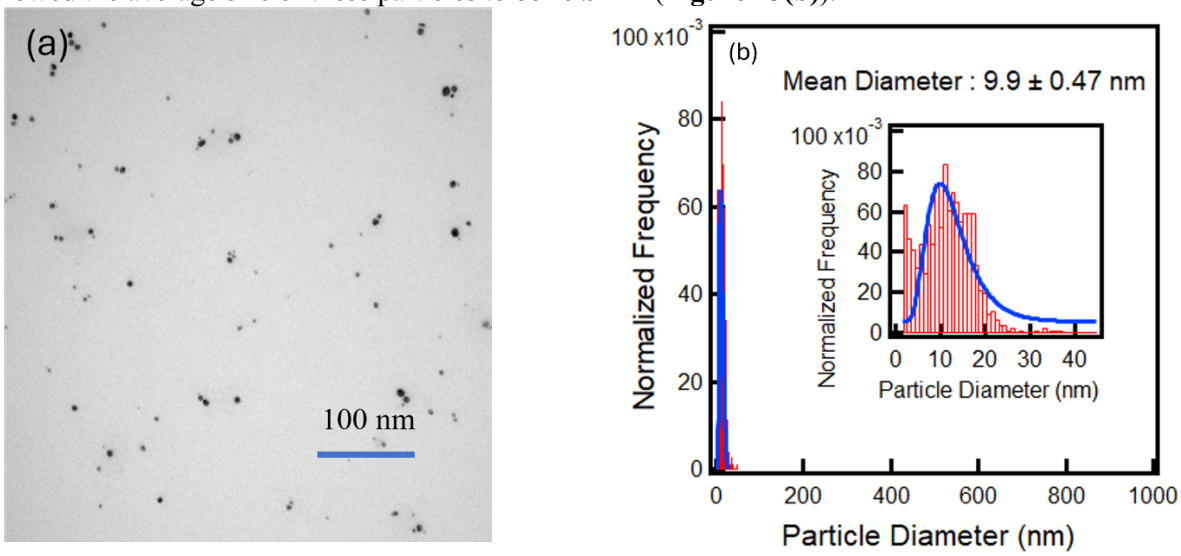

Figure 13. (a) TEM of Cu NPs synthesized in scale-up conditions in JMR. (b) Image J analysis of Cu NPs synthesized in scale-up conditions in JMR.

DLS analysis similarly confirmed a narrow size distribution centered at ~10 nm both from intensity vs. size (**Figure S8**) and number vs. size (**Figure S9**) graph, consistent with results obtained at standard reaction volumes at 100 °C. The superior reproducibility of the JMR could be due to enhanced micromixing capability: the impingement of liquid jets generates rapid and homogeneous mixing,[25] reducing concentration gradients that otherwise lead to localized supersaturation and uncontrolled growth in batch mode. This efficient mixing environment ensures uniform nucleation and suppresses secondary

aggregation, thereby producing NPs with consistent particle size and size distribution even when the production quantity was scaled up.

4. Summary

In this work, we demonstrate a high-temperature Jet Mixing Reactor (JMR) for producing Cu NPs that are uniform in size and shape. Compared to conventional batch synthesis where the particles often grow nonuniformly and agglomerate, the JMR produced small and uniform particles. These observations are based on UV–Vis data, where the batch method produce materials with broad peaks that shift over time. In contrast, the JMR produced materials that had sharp and stable peaks, meaning the particles were monodisperse and reproducible. Even when the precursor volume was scaled up, the JMR still produced NPs around 9–10 nm, the same as with smaller volumes. This was possible because the JMR mixed the solutions quickly and uniformly, leading to uniform nucleation and controlled growth. Overall, the JMR provided a reliable and scalable way to make monodisperse Cu NPs, overcoming the limitations of traditional batch methods.

5. Acknowledgements

6. References

(1) Astruc, D. Introduction: Nanoparticles in Catalysis. *Chem. Rev.* **2020**, *120* (2), 461–463. https://doi.org/10.1021/acs.chemrev.8b00696.

(2) Malik, S.; Muhammad, K.; Waheed, Y. Emerging Applications of Nanotechnology in Healthcare and Medicine. *Molecules* **2023**, *28* (18), 6624. https://doi.org/10.3390/molecules28186624.

(3) Biswas, R.; Alam, M.; Sarkar, A.; Haque, M. I.; Hasan, Md. M.; Hoque, M. Application of Nanotechnology in Food: Processing, Preservation, Packaging and Safety Assessment. *Heliyon* **2022**, *8* (11), e11795. https://doi.org/10.1016/j.heliyon.2022.e11795.

(4) Han, X.; Xu, K.; Taratula, O.; Farsad, K. Applications of Nanoparticles in Biomedical Imaging. *Nanoscale* **2019**, *11* (3), 799–819. https://doi.org/10.1039/c8nr07769j.

(5) Lin, H.; Leng, J.; Fan, P.; Xu, Z.; Ruan, G. Scalable Production of Microscopic Particles for Biological Delivery. *Mater. Adv.* **2023**, *4* (14), 2885–2908. https://doi.org/10.1039/D3MA00021D.

(6) Dong, Z.; Wen, Z.; Zhao, F.; Kuhn, S.; Noël, T. Scale-up of Micro- and Milli-Reactors: An Overview of Strategies, Design Principles and Applications. *Chem. Eng. Sci. X* **2021**, *10*, 100097. https://doi.org/10.1016/j.cesx.2021.100097.

(7) Subraveti, S. N.; Wilson, B. K.; Bizmark, N.; Liu, J.; Prud'homme, R. K. Synthesizing Lipid Nanoparticles by Turbulent Flow in Confined Impinging Jet Mixers. *J. Vis. Exp. JoVE* **2024**, No. 210, e67047. https://doi.org/10.3791/67047.

(8) Johnson, B. K.; Prud'homme, R. K. Chemical processing and micromixing in confined impinging jets. *AIChE J.* **2003**, *49* (9), 2264–2282. https://doi.org/10.1002/aic.690490905.

(9) Liu, Z.; Ramezani, M.; Fox, R. O.; Hill, J. C.; Olsen, M. G. Flow Characteristics in a Scaled-up Multi-Inlet Vortex Nanoprecipitation Reactor. *Ind. Eng. Chem. Res.* **2015**, *54* (16), 4512–4525. https://doi.org/10.1021/ie5041836.

(10) Liu, Z.; Hitimana, E.; Olsen, M. G.; Hill, J. C.; Fox, R. O. Turbulent Mixing in the Confined Swirling Flow of a Multi-Inlet Vortex Reactor. *AIChE J.* **2017**, *63* (6), 2409–2419. https://doi.org/10.1002/aic.15572.

(11) Aimiuwu, G.; Khan, F.; Mualen, D.; Tang, W.-T.; Brunelli, N. A.; Paulson, J. A.; Winter, J. O.; Wyslouzil, B. Experimental and Computational Investigation of Mixing Dynamics in Millifluidic Jet Mixing Reactors. *Chem. Eng. J.* **2025**, *516*, 164078. https://doi.org/10.1016/j.cej.2025.164078.

(12) Holunga, D. M.; Flagan, R. C.; Atwater, H. A. A Scalable Turbulent Mixing Aerosol Reactor for Oxide-Coated Silicon Nanoparticles. *Ind. Eng. Chem. Res.* **2005**, *44* (16), 6332–6341. https://doi.org/10.1021/ie049172l.

(13) Lim, J.-M.; Swami, A.; Gilson, L. M.; Chopra, S.; Choi, S.; Wu, J.; Langer, R.; Karnik, R.; Farokhzad, O. C. Ultra-High Throughput Synthesis of Nanoparticles with Homogeneous Size Distribution Using a Coaxial Turbulent Jet Mixer. *ACS Nano* **2014**, *8* (6), 6056–6065. https://doi.org/10.1021/nn501371n.
(14) Ranadive, P.; Parulkar, A.; Brunelli, N. A. Jet-Mixing Reactor for the Production of Monodisperse Silver Nanoparticles Using a Reduced Amount of Capping Agent. *React. Chem. Eng.* **2019**, *4* (10), 1779–1789. https://doi.org/10.1039/C9RE00152B.
(15) Parulkar, A.; Brunelli, N. A. High-Yield Synthesis of ZIF-8 Nanoparticles Using Stoichiometric Reactants in a Jet-Mixing Reactor. *Ind. Eng. Chem. Res.* **2017**, *56* (37), 10384–10392. https://doi.org/10.1021/acs.iecr.7b02849.
(16) Ranadive, P.; Blanchette, Z.; Spanos, A.; Medlin, J.; Brunelli, N. Scalable Synthesis of Selective Hydrodeoxygenation Inverted Pd@TiO2 Nanocatalysts. *J. Flow Chem.* **2021**, *11*. https://doi.org/10.1007/s41981-021-00171-4.
(17) Ranadive, P.; Khan, F.; O. Winter, J.; Brunelli, N. Dual Jet-Mixing Reactor for Fully Continuous Synthesis of Core@shell Au@Ag Nanocomposites. *React. Chem. Eng.* **2024**, *9* (11), 2915–2924. https://doi.org/10.1039/D3RE00417A.
(18) O'Brien, R. J.; Davis, B. H. Impact of Copper on an Alkali Promoted Iron Fischer–Tropsch Catalyst. *Catal. Lett.* **2004**, *94* (1), 1–6. https://doi.org/10.1023/B:CATL.0000019322.69160.ef.
(19) Camats, M.; Pla, D.; Gómez, M. Copper Nanocatalysts Applied in Coupling Reactions: A Mechanistic Insight. *Nanoscale* **2021**, *13* (45), 18817–18838. https://doi.org/10.1039/D1NR05894K.
(20) Mourdikoudis, S.; Menelaou, M.; Fiuza-Maneiro, N.; Zheng, G.; Wei, S.; Pérez-Juste, J.; Polavarapu, L.; Sofer, Z. Oleic Acid/Oleylamine Ligand Pair: A Versatile Combination in the Synthesis of Colloidal Nanoparticles. *Nanoscale Horiz.* **2022**, *7* (9), 941–1015. https://doi.org/10.1039/D2NH00111J.
(21) Khan, A.; Rashid, A.; Younas, R.; Chong, R. A Chemical Reduction Approach to the Synthesis of Copper Nanoparticles. *Int. Nano Lett.* **2016**, *6* (1), 21–26. https://doi.org/10.1007/s40089-015-0163-6.
(22) Mott, D.; Galkowski, J.; Wang, L.; Luo, J.; Zhong, C.-J. Synthesis of Size-Controlled and Shaped Copper Nanoparticles. *Langmuir* **2007**, *23* (10), 5740–5745. https://doi.org/10.1021/la0635092.
(23) *Cu and Cu-Based Nanoparticles: Synthesis and Applications in Catalysis | Chemical Reviews*. https://pubs.acs.org/doi/10.1021/acs.chemrev.5b00482 (accessed 2023-06-23).
(24) Aissa, M. A. B.; Tremblay, B.; Andrieux-Ledier, A.; Maisonhaute, E.; Raouafi, N.; Courty, A. Copper Nanoparticles of Well-Controlled Size and Shape: A New Advance in Synthesis and Self-Organization. *Nanoscale* **2015**, *7* (7), 3189–3195. https://doi.org/10.1039/C4NR06893A.
(25) Aimiuwu, G.; Khan, F.; Mualen, D.; Tang, W.-T.; Brunelli, N. A.; Paulson, J. A.; Winter, J. O.; Wyslouzil, B. Experimental and Computational Investigation of Mixing Dynamics in Millifluidic Jet Mixing Reactors. *Chem. Eng. J.* **2025**, *516*, 164078. https://doi.org/10.1016/j.cej.2025.164078.

Synthesis of Cu NPs in a high-temperature jet mixing reactor

Supplemental Information

Authors: Priya Jana,[a] and Nicholas A. Brunelli*[,a]

Author address: [a] The Ohio State University, William G. Lowrie Department of Chemical and Biomolecular Engineering, 151 W. Woodruff Ave., Columbus, OH 43210, U.S.A.0

***Corresponding author**: Email: brunelli.2@osu.edu; Twitter: OSUChemEProfBru

Fits and FWHM for batch synthesis of Cu NPs in different runs

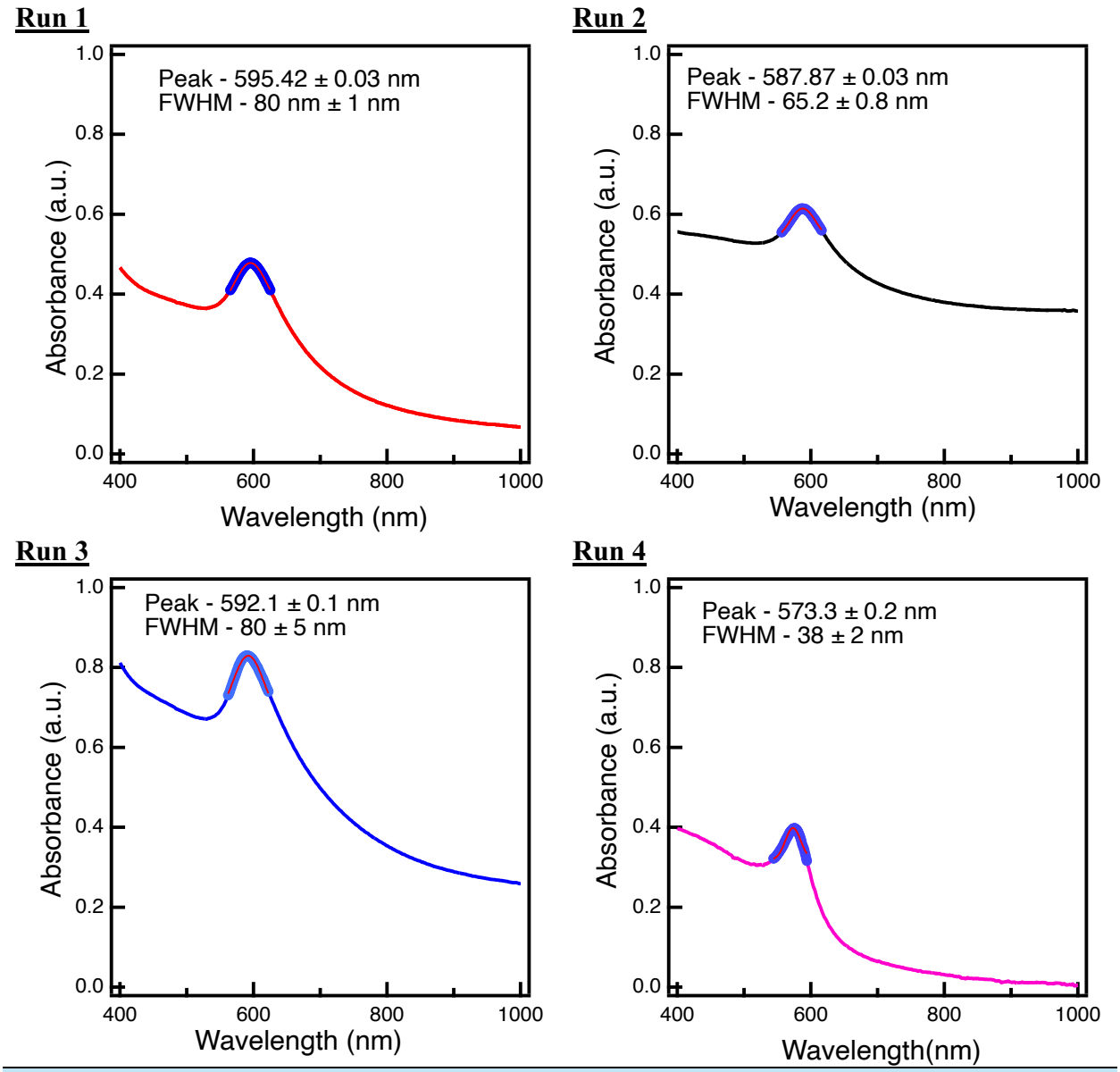

Figure S1. UV-vis data for different batch runs and the gaussian fits from Igor.

Table S1. The variability in the properties of the surface plasmon resonance (i.e. absorbance,wavelength of maximum absorbance, and full width at half maximum (FWHM) measured by UV-VIS for four different batch runs used to plot Figure 8

Run no	**Absorbance**	**Wavelength of max abs (nm)**	**FWHM (nm)**
1	0.31	595	80
2	0.61	587	65
3	0.83	592	80
4	0.48	573	38
Average	*0.56±0.22*	*587±10*	*67±20*

Fit and FWHM for JMR synthesis of Cu nps in different runs

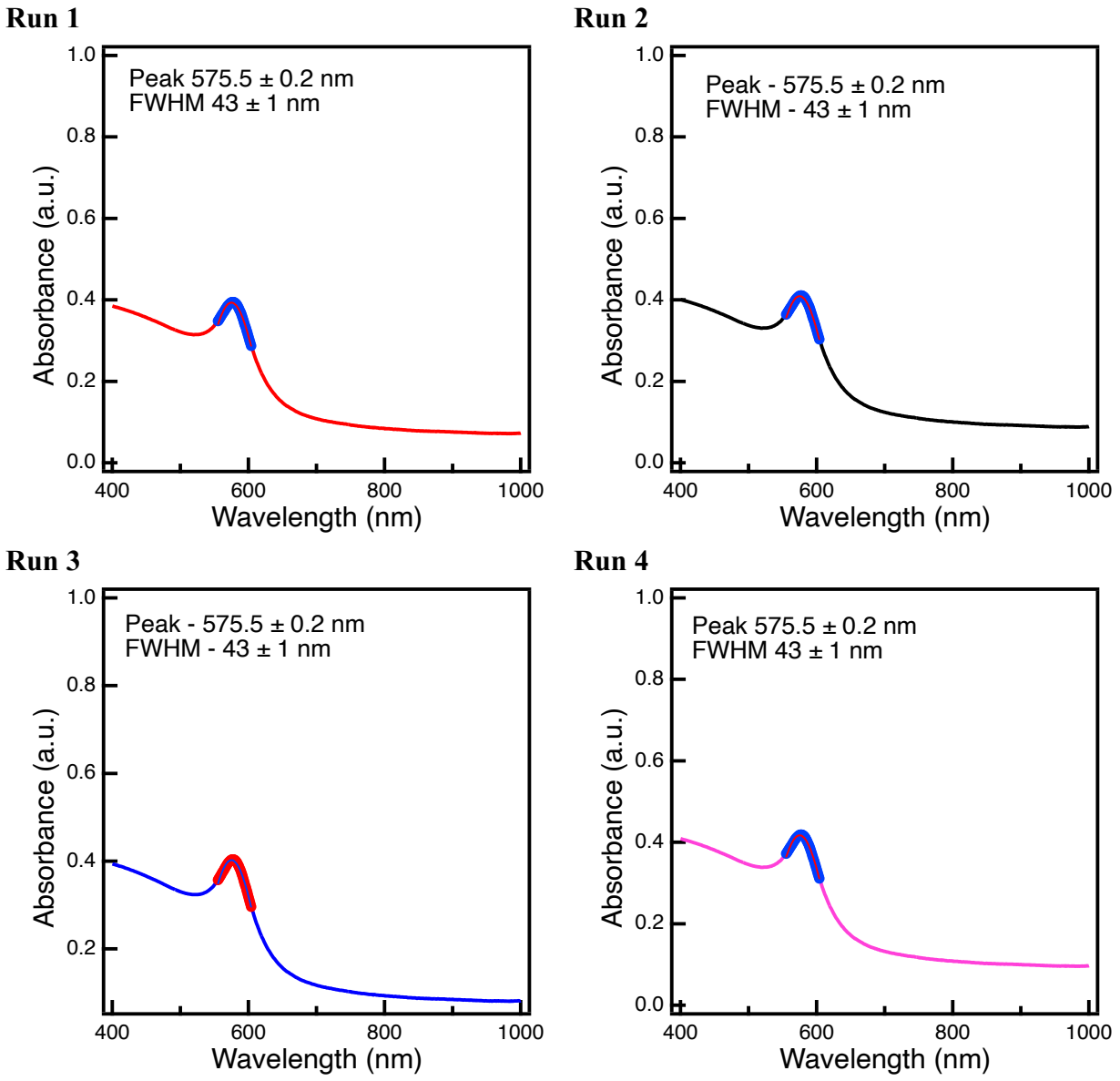

Figure S2. UV-vis data for different JMR runs and the gaussian fits from Igor.

Table S2. The variability in the properties of the surface plasmon resonance (i.e. absorbance,wavelength of maximum absorbance, and full width at half maximum (FWHM) measured by UV-VIS for four different Jet mixing reactor runs used to plot Figure 8

Run no	Absorbance	Wavelength of max abs (nm)	FWHM (nm)
1	0.069 ± 0.002	575.5±0.2	43±1
2	0.069 ± 0.002	575.5±0.2	43±1
3	0.069 ± 0.002	575.5±0.2	43±1
4	0.069 ± 0.002	575.5±0.2	43±1
Average	*0.069*	*575*	*43*

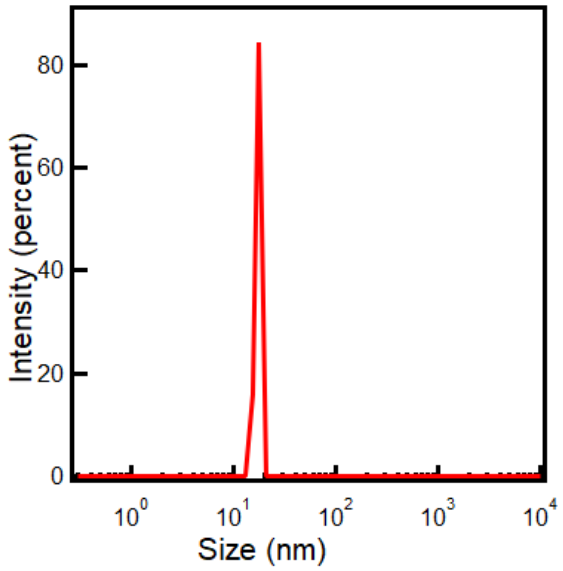

Figure S3. Intensity vs. size graph of Cu NPs synthesized in JMR at 100 °C at Q_{main} = 0.4 mL min^{-1} and Q_{jet} = 0.2 mL min^{-1}.

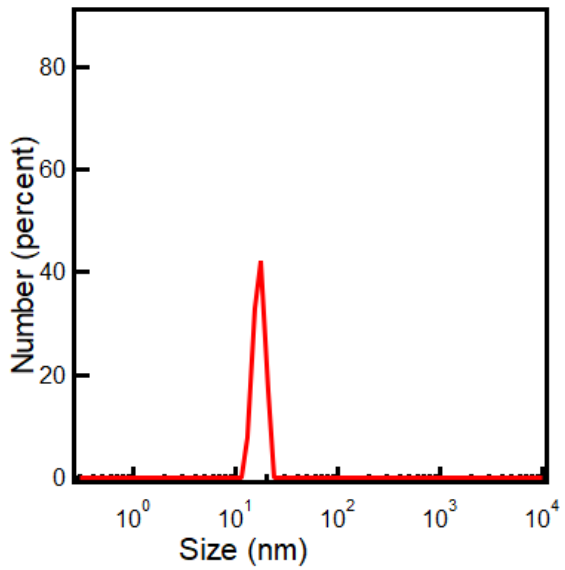

Figure S4. Intensity vs. size graph of Cu NPs synthesized in JMR` at 100 °C at Q_{main} = 0.4 mL min^{-1} and Q_{jet} = 0.2 mL min^{-1}.

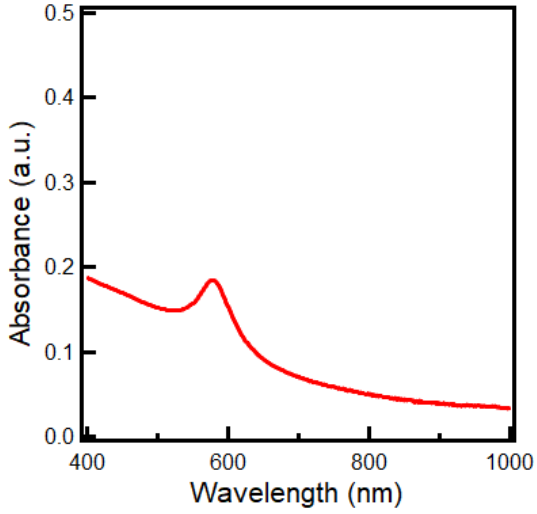

Figure S5. UV-Vis spectrum of Cu NPssynthesized in JMR at 100 °C at Q_{main} = 0.8 mL min^{-1} and Q_{jet} = 0.4 mL min^{-1} under modified conditions.

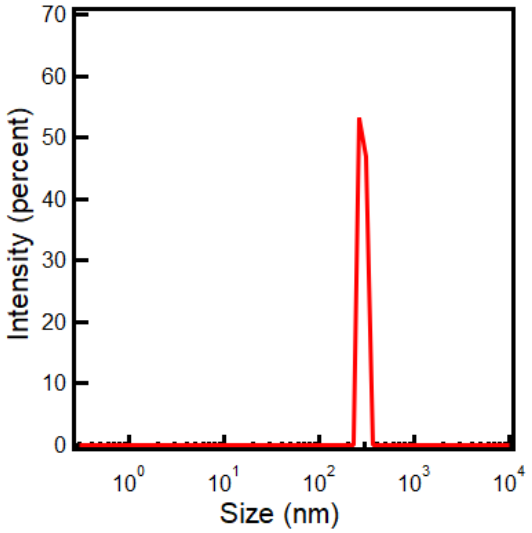

Figure S6. Intensity vs. size graph of Cu NPs synthesized in the JMR at 80 °C.

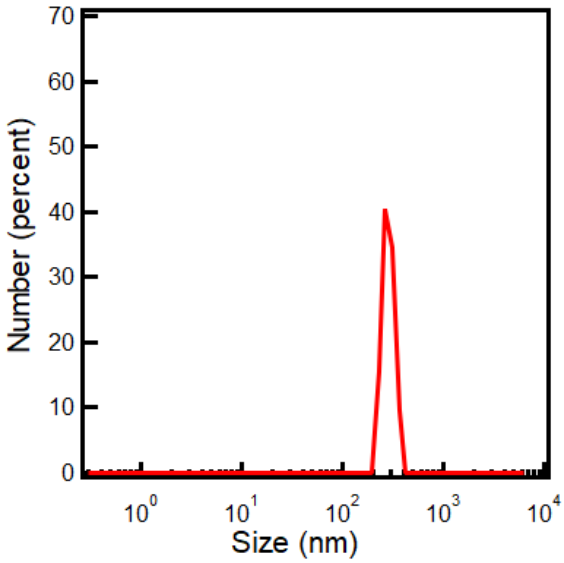

Figure S7. Intensity vs. size graph of Cu NPs synthesized in the JMR at 80 °C.

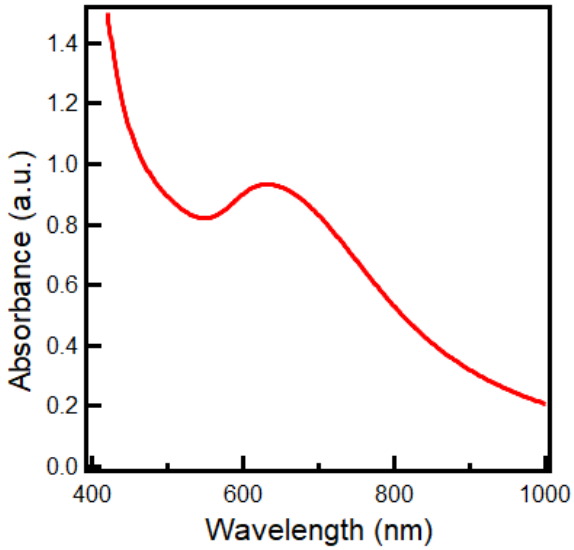

Figure S8. UV-Vis spectrumof Cu NPs synthesized in batch at 100 °C under scaled up conditions

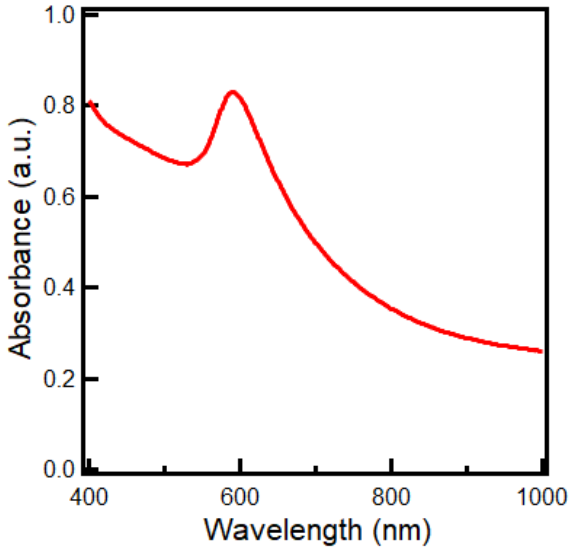

Figure S9. UV-Vis spectrum of Cu NPs synthesized in JMR at 100 °Cunder scaled up conditions

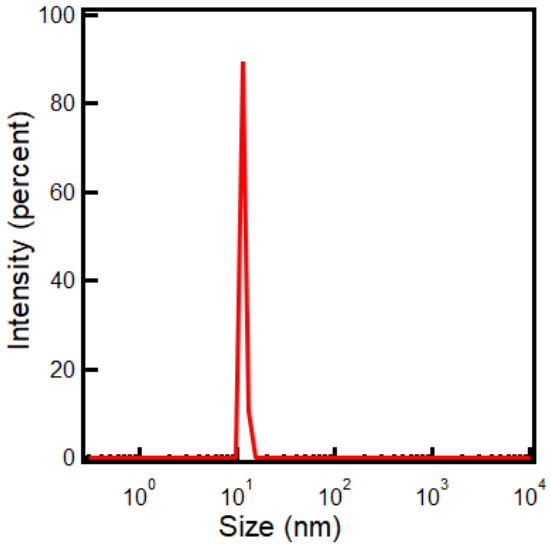

Figure S10. Intensity vs. size graph of Cu NPs synthesized in JMR at 100 °C under scaled up conditions.

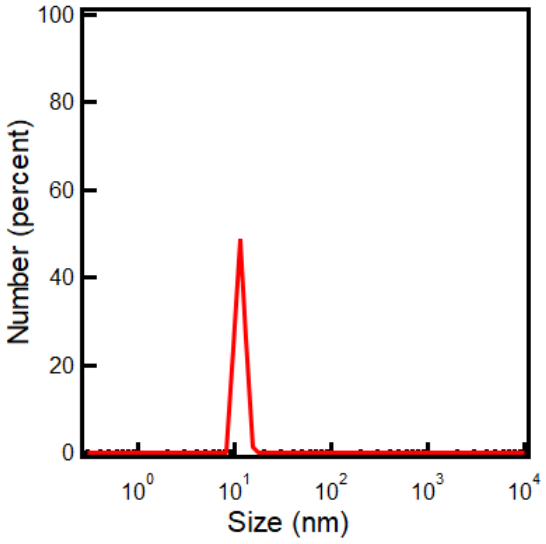

Figure S11. Number vs. size graph of Cu NPs synthesized in JMR at 100 °C under scaled up conditions.